/V/l5 7- /00

7/V -32- /2/

0 2/260

A Satellite-Tracking *K*- and K_a-Band

Mobile Vehicle Antenna System

Arthur C. Densmore
Vahraz Jamnejad

A Satellite-Tracking K- and K_a-Band Mobile Vehicle Antenna System

Arthur C. Densmore, *Member, IEEE,* and Vahraz Jamnejad, *Member, IEEE*

Abstract— This paper describes the development of the K- and K_a-band, satellite-tracking mobile-vehicular antenna system for NASA's ACTS Mobile Terminal (AMT) project. ACTS is NASA's Advanced Communications Technology Satellite, which will be launched into its geostationary orbit in September 1993. The AMT task will make the first experimental use of the satellite soon after the satellite is operation, to demonstrate mobile communications via the satellite from a van on the road. The AMT antenna system consists of a mechanically steered small reflector antenna that uses a shared aperture for both frequency bands and fits under a radome of 23 cm diameter and 10 cm height, and an antenna controller that tracks the satellite as the vehicle moves about. The RF and mechanical characteristics of the antenna and the antenna tracking control system are discussed. Laboratory measurements of the antenna performance are presented.
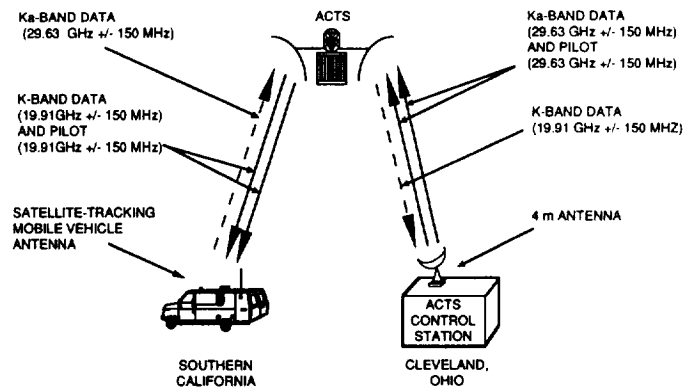
Fig. 1. Overall AMT experiment setup.

I. INTRODUCTION

THE Jet Propulsion Laboratory (JPL) has developed several mobile vehicular antenna systems for satellite applications [1]–[16]. JPL has installed these antenna systems in vehicles equipped as mobile communications laboratories [17], [18] and field tested the equipment. The results of the field trials have been documented in the literature [19]–[24].

Recently a K- and K_a-band mobile vehicle antenna system has been developed by JPL for use with NASA's Advanced Communications Technology Satellite (ACTS). The ACTS satellite was launched into its geostationary orbit at 100° West longitude (above the mid-western United States) in September 1993. The new mobile vehicle antenna development is the ACTS Mobile Terminal (AMT) reflector antenna system. Soon after the satellite is operational, the AMT project will demonstrate the first experimental use of ACTS, with direct-dial voice, video, and data communications from a mobile vehicle while traveling in the southern California area [25]. All communications will be via a digital link, utilizing data rates up to 64 kbps.

The AMT experiment setup is shown in Fig. 1. The AMT will initially operate in the Los Angeles area and communicate via ACTS with the ACTS master control ground station at the NASA Lewis Research Center in Cleveland, Ohio. The AMT will utilize the ACTS Los Angeles/San Diego spot beam. ACTS translates the Cleveland K_a-band (30 GHz) uplink signals to K-band (20 GHz) and relays them down to the AMT in southern California. The Cleveland ground station is
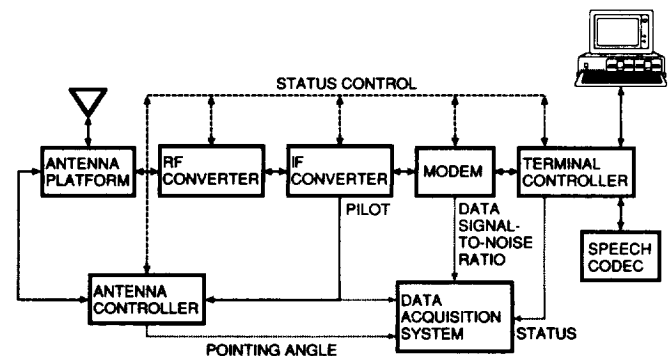
Fig. 2. AMT equipment block diagram.

required to continuously transmit a pilot tone whether or not it sends a data signal, both at K_a-band. The AMT requires the pilot tone to track the satellite with its antenna. (One pilot tone would be used by all mobile terminals for satellite tracking in a multiple-user ACTS system.) ACTS translates the AMT K_a-band uplink signal to K-band and relays it to the Cleveland ground station.

The method the AMT reflector antenna system uses for satellite tracking involves "mechanical dithering" of the antenna. The antenna is smoothly rocked (dithered) side-to-side through a small angle (1°) while the signal strength of the pilot tone received through the antenna is monitored; this allows the antenna controller computer to determine if the antenna is pointed in the direction of the strongest signal. The mechanical dithering causes less than 0.3 dB and 0.2° fluctuation of the signals. The satellite tracking system is discussed in greater detail later.
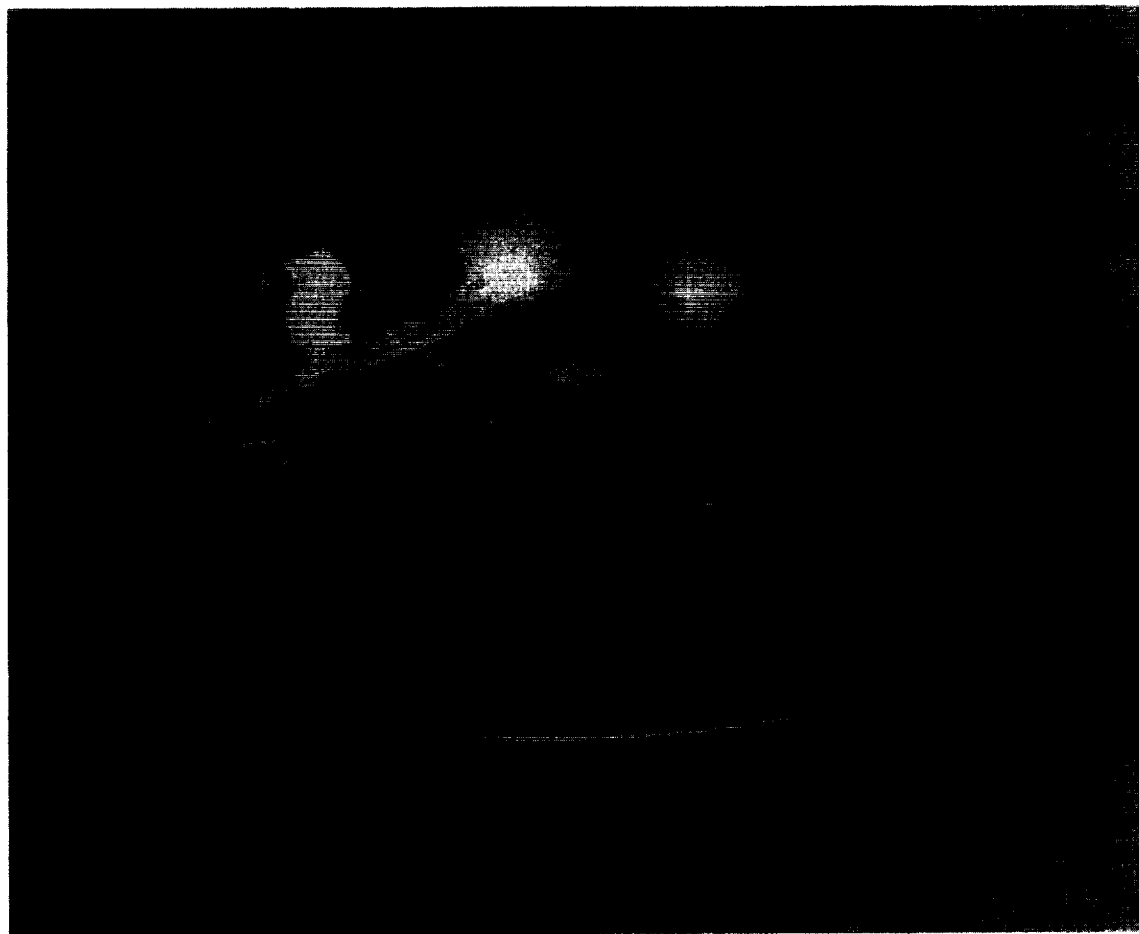
Fig. 3. AMT reflector antenna assembly.

The overall AMT system is summarized by the equipment block diagram of Fig. 2. The antenna system consists of the antenna assembly and the antenna controller computer. The antenna assembly mounts onto the roof of the AMT vehicle, and the antenna controller computer installs inside the vehicle with the other AMT equipment. In addition to the reflector antenna system, the AMT includes high-performance RF up- and down-converters, a robust digital modem, capable of multiple data rates for rain-compensation, a speech encoder/decoder (codec) to communicate voice through the digital communications link, a terminal controller computer which orchestrates the operation of the entire AMT, and a data acquisition system which simultaneously records all critical system parameters while also displaying the status of any selected subsystem in real-time. The entire AMT will be installed in a van for the first experiments and into a sedan for later demonstrations.

Development of K_a-band antenna technology is one of the key objectives of the AMT project. The benefits of K_a-band include a much larger available bandwidth, higher antenna gain and/or a substantial size reduction compared to lower frequency bands [26]. Reaping these benefits requires overcoming disadvantages of higher RF component losses, significant rain attenuation [27], higher Doppler (up to 3 KHz at K_a-band) and the need for a more accurate satellite-tracking
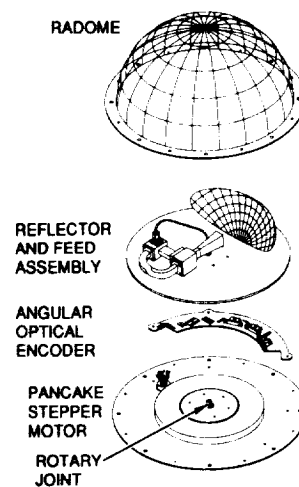

Fig. 4. Exploded view of antenna.

system to accommodate a narrower (higher gain) antenna beam. The AMT design overcomes these disadvantages. The following requirements for the reflector antenna system ensure a high level of performance for the overall AMT system.

The AMT reflector antenna system satisfies the following requirements: 1) The antenna system shall be rugged enough to withstand the shock and vibration of the mobile vehicle
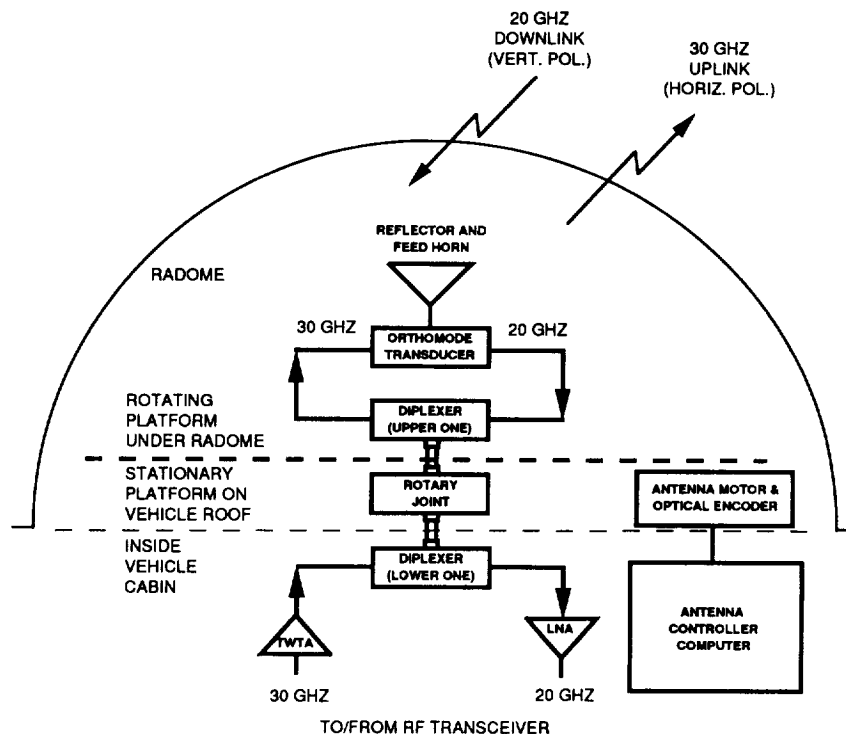
Fig. 5.   Antenna block diagram.

environment. 2) The antenna shall complete a full azimuth search and acquire the satellite signal within 10 s. 3) The antenna system shall track the satellite by compensating for vehicle turn (yaw) rates up to 45°/s and vehicle pitch and roll up to ±6°,) The satellite tracking system shall not lose track of the satellite direction during signal outages of up to 10 s. (It must rely on inertial pointing during such periods.) 5) The antenna system shall provide a minimum of 20.5 dB isotropic gain for transmission at 29.63 ± 0.15 GHz and handle up to 10 W transmit power. 6) The antenna system shall provide a minimum gain to noise-temperature ratio (G/T) of -8 dB/K over the receive band of 19.91 ± 0.15 GHz. 7) The antenna shall have minimal cross-polarization and sidelobe levels no greater than -13 dB.

II. ANTENNA ASSEMBLY

The antenna installs on the roof of the AMT vehicle. Fig. 3 is a picture of the AMT reflector antenna shown with a transparent mock radome; the actual radome has the same shape but is opaque. The external dimensions of the radome are 23 cm in diameter and 10 cm in peak height. A coaxial connector at the center of the underside of the antenna is the sole RF connection that carries both transmit and receive signals between the antenna and the AMT RF equipment installed inside the vehicle. A second connector on the underside brings power for the antenna's motor and returns signals from an optical encoder which reports the motor angle.

Fig. 4 is an exploded view of the antenna assembly. The reflector and feed horn mount to a disk that attaches directly to the motor for azimuth steering. Below the disk an optical encoder monitors the disk angle to verify that the motor steers

the antenna to the commanded angle. The optical encoder has three infrared reflective switches (sensors) that respond to a reflective optical wheel decal installed on the underside of the disk. Two of the sensors report incremental angle in quadrature (sin/cos), and the third sensor simply reports when the motor angle equals zero. A coaxial rotary joint mounts in the center of the motor and distributes RF signals to the components on the disk.

A. RF Characteristics:

Fig. 5 is a functional block diagram of the antenna. The ACTS Los Angeles/San Diego spot beam downlink (20 GHz) is vertically polarized, and the uplink (30 GHz) is horizontally polarized. The AMT reflector antenna uses a single reflector and feed horn for both uplink and downlink. The two frequency bands also share a single-channel coaxial rotary joint for RF distribution between the rotating and stationary antenna components. A low-noise amplifier (LNA) and traveling-wave tube amplifier (TWTA) are mounted within the vehicle cabin below the antenna to establish the required receive sensitivity and provide the transmit RF power, respectively. A thin but sturdy radome protects the antenna from the outside environment.

1) Overall Performance: Fig. 6 presents the measured elevation and azimuth co- and cross-polarization 20 and 30 GHz patterns of the overall antenna, including the radome. The patterns show the elevation coverage centered at 46°, the ACTS elevation look angle in Los Angeles. The elevation coverage can be manually adjusted from 30–60° (the range of elevation look angle for ACTS across the continental United States). The antenna is designed to operate over a 12° elevation

Elevation Pattern, 20 GHz, Co- and X-pol.

Elevation Pattern, 30 GHz, Co- and X-pol.

Azimuth Pattern, 20 GHz, Co- and X-pol.

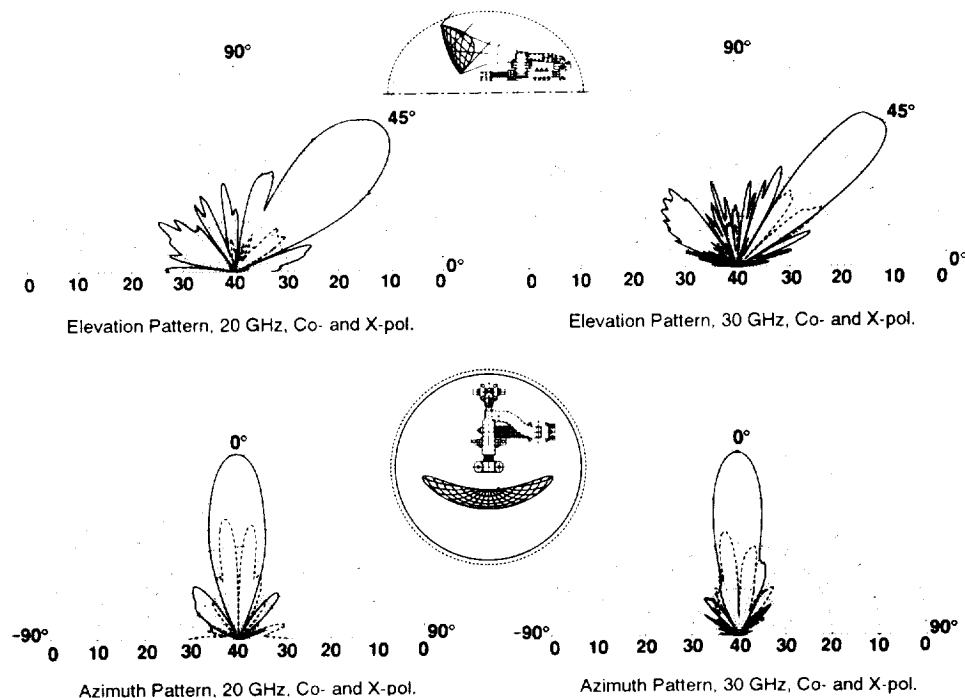Azimuth Pattern, 30 GHz, Co- and X-pol.

Fig. 6.   Far-field pattern measurements.

range centered about any manual setting within the 30–60° range and is optimized for operation in the Los Angeles area. The 12° range accommodates typical vehicle pitch and roll variation while driving.

Over the 12° elevation range, when set for operation in Los Angeles, the transmit gain (30 GHz) is a minimum of 20.8 dBi with a peak of 23.5 dBi, and the receive gain (20 GHz) is a minimum of 19.5 dBi with a peak of 23.0 dBi. Antenna gain is measured at the bottom of the rotary joint. (These gain values reduce by about 0.7 dB when the elevation angle is manually adjusted to the extremes of 30 or 60°.) The elevation and azimuth sidelobes are more than 20 dB down from the main lobe. Peak cross-polarization is no greater than −15 dB. The variation of antenna gain as a function of frequency within the receive and transmit 300 MHz bands is shown in Fig. 7. The gain variation is within ±0.5 dB for both bands. Within the same 300 MHz bands the sidelobe and cross-polarization levels do not vary more than ±0.5 dB from those shown in Fig. 6.

The minimum receive system G/T is better than −6 dB/K over the 12° elevation range. The receive system noise temperature, referenced to the bottom of the rotary joint, is 335 K. (The noise figure of the LNA is 2.5 dB.) When pointed directly at the sun the receive system noise temperature increases by only 0.1 dB (5K). There is no receive sensitivity degradation (±0.05 dB) when simultaneously transmitting at the maximum power level of 10 W.

2) Reflector: The antenna incorporates an offset reflector configuration to avoid feed horn aperture blockage. The reflector is constrained to fit with the feed horn under the radome and is relatively small, only about 4 by 10 wavelengths at *K*-band. The basically elliptical reflector shape maximizes gain while providing a relatively wide elevation beamwidth to relax the
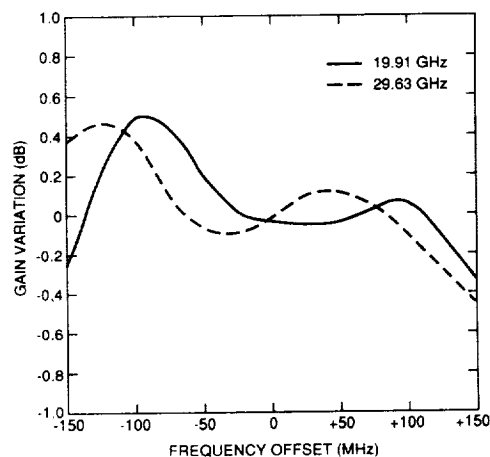

Fig. 7.   Gain frequency response.

need for satellite elevation tracking. The shape of the reflector is the intersection of a paraboloid and an elliptical cylinder, with the cylinder oriented so the projection of the reflector surface is nearly a simple ellipse as viewed from both the feed horn and the satellite directions; this orientation is important to ensure both good illumination of the reflector by the feed horn and a reasonably symmetrical antenna elevation pattern. It also contours the shape of the reflector to fit well under the radome. The focal-length-to-diameter ratio (F/D) in the elevation plane is about 0.7, and in the azimuth plane about 0.3.

The reflector mounts to a manually adjustable fixture which sets the elevation angle of the antenna beam within the range of 30–60°. (A greater elevation angle range can be accommodated by modifying the fixture.) The angle of the reflector adjusts while the feed horn remains stationary, and for any setting in this range there is no mechanical interference with
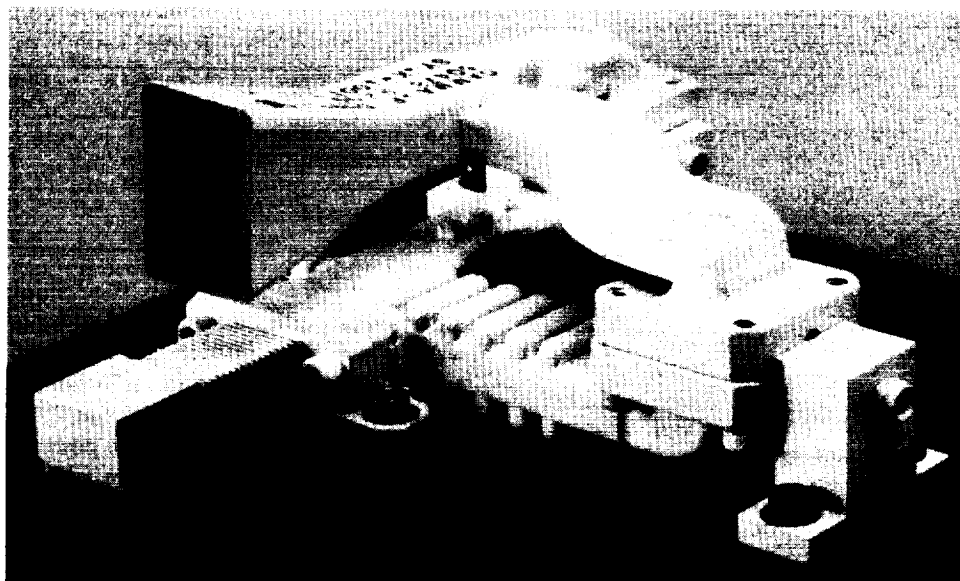
Fig. 8.   Feed horn assembly.

the radome. To afford the ±15° (30–60) elevation adjustment the reflector mounting fixture only has to adjust approximately ±8°. This accounts for both the basic principle of reflection when the angle of the reflecting surface varies (a factor of 2) as well as the beam deviation factor for this antenna (about 0.95 with the 0.7 F/D ratio in the elevation plane) [28].

3) Feed Horn Assembly: All of the antenna RF components are integrated into a single rigid assembly, except for the reflector and rotary joint, to reduce RF losses and increase the mechanical integrity. Fig. 8 shows the feed horn, orthomode transducer and upper diplexer (the components above the rotary joint in Fig. 5) all integrated into a single feed horn assembly. The feed horn assembly is a waveguide system that distributes both the 20 and 30 GHz signals from the rotary joint to the feed horn. The one feed horn is used for both frequency bands, with vertical polarization for the 20 GHz downlink and horizontal polarization for the 30 GHz uplink. Immediately behind the feed horn is the orthomode transducer. The orthomode transducer combines the two frequency bands from two different ports and channels them to the feed horn after orienting them with the proper polarizations. The upper diplexer spatially separates the two frequency bands and distributes them to the respective ports of the orthomode transducer. The diplexer makes up most of the lower portion of the assembly and consists of a tee-junction of a lowpass filter for 20 GHz and a highpass filter for 30 GHz. The feed horn assembly also includes a coax-to-waveguide transition, to adapt directly to the coaxial rotary joint connector, and a section of flexible waveguide that connects the coax transition to the rest of the waveguide structure and accommodates any misalignment of the rotary joint and motor axes as the motor turns. The RF losses through the feed horn assembly are about 0.2 dB at 20 GHz and 0.4 dB at 30 GHz.

4) Rotary Joint: The rotary joint distributes the RF signals from the stationary motor base to the antenna components turned by the motor and provides the sole RF connection on

the underside of the antenna. It is a single-channel coaxial unit, and as such is a relatively small unit that imposes a minimum of frictional torque—less than 0.035 N · m. The rotary joint is only 1.3 cm in diameter and installs in the very center of the motor assembly. The choice of such a small rotary joint is a major factor in achieving the overall reduction in size of the antenna. The RF loss through the rotary joint is about 0.5 dB at both 20 and 30 GHz.

5) Diplexer: A second (lower) diplexer, diagrammed in Fig. 5, connects to the antenna's RF connector (at the bottom of the rotary joint) and connects the transmitter and receiver to the antenna. The lower diplexer is a separate unit but is of the same design as the upper diplexer in the feed horn assembly. The RF insertion loss of the diplexer is about 0.2 dB at 20 GHz and 0.3 dB at 30 GHz. A 20 GHz LNA with a 2.5 dB noise figure and 25 dB of gain connects to the lower diplexer and helps satisfy the receive G/T requirement. A TWTA also connects to the lower diplexer and supplies the 1 W 30 GHz signal to the antenna required for nominal AMT uplink communications. The return loss measured at the two external ports of the lower diplexer represents the impedance match of the entire RF system of Fig. 5. These measurements, of the 20 and 30 GHz diplexer ports respectively, are shown in Fig. 9. The VSWR in the 30 GHz frequency band is better than 1.5:1. Over most of the 20 GHz band the VSWR is better than 1.5:1; although, in the lower 20% of the frequency band the VSWR approaches 2:1.

6) Radome: The radome is 3.5 mm thick and of an "A-sandwich" layered design, formed into a hemi-ellipsoidal shape—23 cm in diameter and 10 cm in height. It is designed to withstand 250 km/h winds. The radome is painted with a polyurethane sealant and coated with a hydrophobic coating that is nearly electromagnetically transparent and keeps water from wetting the radome surface. The hydrophobic coating helps the AMT maintain communications in light rain. Comparison of antenna measurements with and without the radome
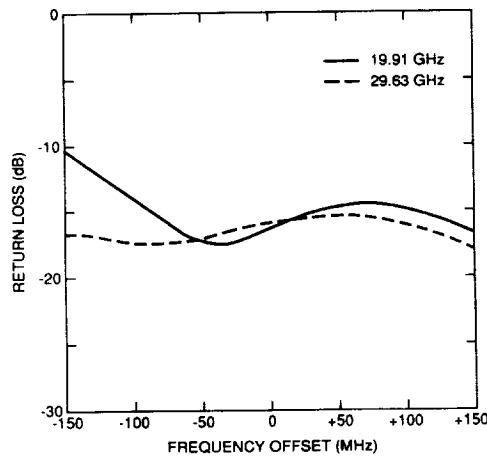
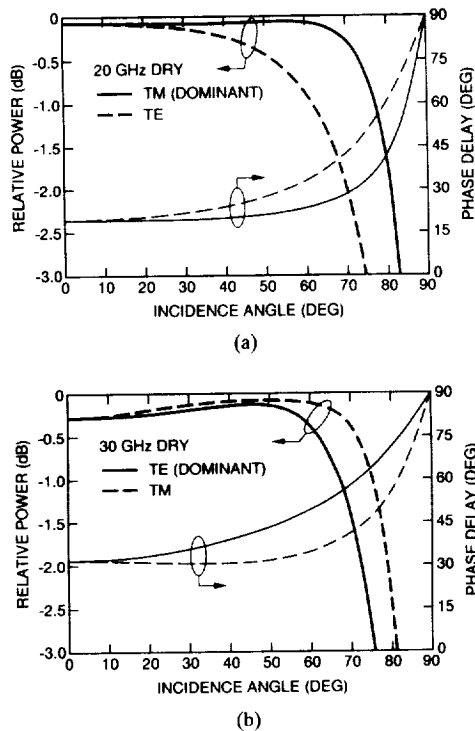Fig. 9. System return loss, at lower diplexer ports.

(a)

(b)

Fig. 10. Analysis of flat radome with hydrophobic coating.

TABLE I
RADOME LAYERS

Radome Layer	Thickness (mm)	Dielectric Constant	Loss Tangent
Hydrophobic coating	0.150	1.0	0.001
Polyurethane paint	0.076	3.3	0.030
Quartz epoxy	0.254	3.4	0.006
Honeycomb spacer	2.794	1.1	0.003
Quartz epoxy	0.254	3.4	0.006

reflection properties for an individual layer. By multiplying the wave transmission matrices for all of the layers, the overall radome transmission matrix is obtained, which completely characterizes the multilayer radome.

Fig. 10 shows the transmission power loss and phase delay for the 20 and 30 GHz bands for both senses of polarization as functions of the incidence angle of a plane wave with a flat radome. TE polarization is defined as the incident electric field vector being transverse to the radome surface normal vector. TM polarization is defined as the incident magnetic field vector being transverse to the radome surface normal vector. For small incidence angles there is little distinction between TE and TM orientations. The TM polarization sense dominates at 20 GHz, and TE at 30 GHz; this is because the AMT 20 GHz downlink is vertically polarized, and the 30 GHz uplink horizontally polarized. Since the radome is not flat but curved, the incidence angle of the wave front on the local radome surface varies. The variation of the incidence angle is about 25 to 65° across the reflector aperture projected onto the radome with the reflector set to accommodate a satellite elevation look angle of 46°. For different elevation angle settings the incidence angle range is different. In Fig. 10(a) (20 GHz dry, flat radome analysis) over the 25 to 65° range the average TM transmission loss is 0.1 dB, and the variation in TM transmission phase no more than 5°. In Fig. 10(b) (30 GHz dry, flat radome analysis) over the 25 to 65° range the average TE transmission loss is 0.3 dB, and the variation in TE transmission phase is about 20°. This analysis of transmission loss agrees very well with the measurements (0.2 dB at 20 GHz and 0.4 dB at 30 GHz). The measurement of a small elevation beam squint caused by the radome at 30 GHz but not at 20 GHz also agrees with the analysis, in that the variations in both transmission loss and phase are seen in Fig. 10 to be much more significant at 30 GHz than at 20 GHz. (Distortion of the aperture field magnitude and phase distribution distorts the far-field antenna pattern.)

A comparison of Figs. 10 and 11 reveals how the radome hydrophobic coating helps the AMT maintain communications in light rain. (During heavy or even moderate rain the AMT cannot operate because of the severe signal attenuation caused by clouds at K- and K_a-bands.) In Fig. 11 the same radome structure is analyzed as in Fig. 10, but with the hydrophobic coating layer replaced with a thin, uniform coat of water on the exterior radome surface. The layer of water is conservatively characterized for this analysis by a thickness of 0.025 mm, a dielectric constant of 29, and a loss tangent of 1.03. Without a hydrophobic coating the radome surface could very readily be coated with an even thicker coat of water in a light rain.

reveal that the radome imposes effective transmission losses of 0.2 dB at 20 GHz and 0.4 dB at 30 GHz. Measurements also reveal a 1° elevation beam squint caused by the radome in the 30 GHz band, but no beam squint is observed in the 20 GHz band. These measurements agree with an analysis of a flat version of the radome, presented in Fig. 10. The layers of the radome structure, including the paint and hydrophobic coating, have the electromagnetic characteristics given in Table I.

In order to analyze the transmission and reflection properties of a general, multilayered radome, a computer program was developed, written in MATLAB; a copy may be obtained free of charge by contacting the authors of this article. The program is based on the theoretical formulation presented in [29], [30]. Each layer of the radome is first characterized by a wave transmission matrix which specifies the transmission and
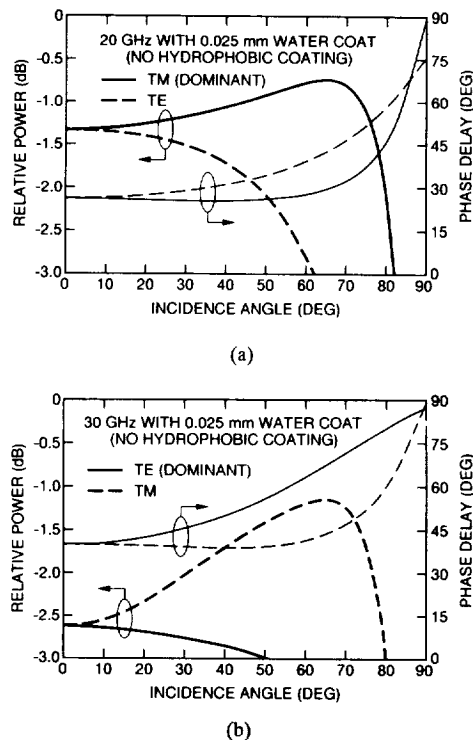
(a)

(b)

Fig. 11. Analysis of flat radome with 0.025 mm coat of water (no hydrophobic coating).

In Fig. 11 the transmission loss at both frequencies with the thin layer of water on the radome is seen to be much greater than that of the dry radome in Fig. 10. With the 0.025 mm coat of water the average radome transmission loss is 1 dB at 20 GHz, and 3 dB at 30 GHz. With twice as thick a coat of water, the losses rise to about 2 dB and 5 dB. In addition to the ability to repel water, the criteria for the selection of a hydrophobic coating included the ability to survive the smog encountered in the Los Angeles area. Outdoor exposure tests eliminated one commercial coating under consideration when it lost its hydrophobic property after one month, thought to be due to hydrocarbon pollutants in the air.

B. Mechanical Characteristics:

An effort has been made to yield an antenna mechanical design which provides both substantial size reduction and enough durability to endure the mobile vehicle environment. This section discusses the basic aspects of the mechanical design of the AMT reflector antenna. The motor design and motor torque requirements are discussed, followed by a discussion of the motor bearings.

1) Motor: The function of the motor is to turn the antenna in azimuth about the vehicle yaw axis. The total mass of all the antenna components rotated by the motor is 670 g. These components include the disk (140 g), reflector (110 g), adjustable reflector mount (110 g), feed horn assembly (255) and ballast (55 g). It is expected that the mass of these components could be significantly reduced during the process of commercial development.

The motor is custom designed for miniaturization and durability. It is a direct-drive, two-phase stepper motor with

a 2° full-step angle and provides 0.21 N · m of holding torque. The choice of a pancake design reduces the motor height to 1.3 cm. The motor has a hole through its center which accommodates the RF rotary joint, and its rotor directly supports the load of the antenna, so no additional space is required for gears. The motor stator coil housings are securely riveted to the motor base rather than spot welded to reduce the effects of fatigue failure and improve corrosion resistance at the attachment points. Materials for the motor were specifically selected for improved linearity so the motor would perform well with a microstepping motor driver. With the use of an 8-bit microstepping motor driver nearly continuous angular resolution is achieved for precise antenna azimuth steering, accurate to 0.05°.

2) Motor Torque: At a minimum the motor has to have sufficient torque to overcome the friction in the antenna assembly. Since the antenna tracks a very distant geostationary satellite, the antenna essentially does not turn (inertially) while the vehicle, to which it mounts, turns underneath it. Torque is also required for the mechanical dithering process and for accelerating the antenna on command; e.g., spinning through a full azimuth rotation to search for the satellite during an acquisition procedure. In addition, sufficient holding torque is required to keep the antenna azimuth angle natural frequency well above the mechanical dithering frequency so the natural response does not interfere with the tracking system response. A motor torque of 0.14 N · m is sufficient to satisfy these requirements, and the motor provides 0.21 N · m.

The available motor torque and rotational inertia of the antenna minimize the mechnical dithering rate that can be used for satellite tracking. It is also desirable to minimize the dither rate to minimize vibration within the antenna. Yet it is desirable to maximize the dither rate to maximize the bandwidth of available antenna tracking information obtained by the mechnical dithering process. Accounting for inertia and friction, about 0.021 N · m of peak torque is required to dither the antenna 1° in each direction at a 2 Hz rate. The 2 Hz rate has provided good performance in laboratory tests.

3) Bearings: The mobile-vehicle application dictates that causes of decreased motor bearing life be addressed to maximize the life of the antenna. Such causes of reduced bearing life include misalignment, play, and insufficient hydrodynamic lubrication. These causes are addressed in the motor design. To minimize misalignment, all components are registered radially to the motor bearings. In particular, registration of the rotary joint is essential so that it won't oppose the motor bearings as the motor turns the antenna. Play is minimized with the use of a pair of angular contact bearings in a DB duplex configuration. With angular contact bearings in this configuration, the effective distance between the pair of bearing is greater than the actual distance, which allows the overall thickness of the motor to be reduced and creates a very rigid bearing support that minimizes both axial and radial deflections. The duplexed angular contact bearing pair also allows higher moment loads than comparable deep groove bearing pairs, while allowing high thrust loads. Insufficient hydrodynamic lubrication is a concern because the small-amplitude (1°) mechanical dithering of the antenna operates
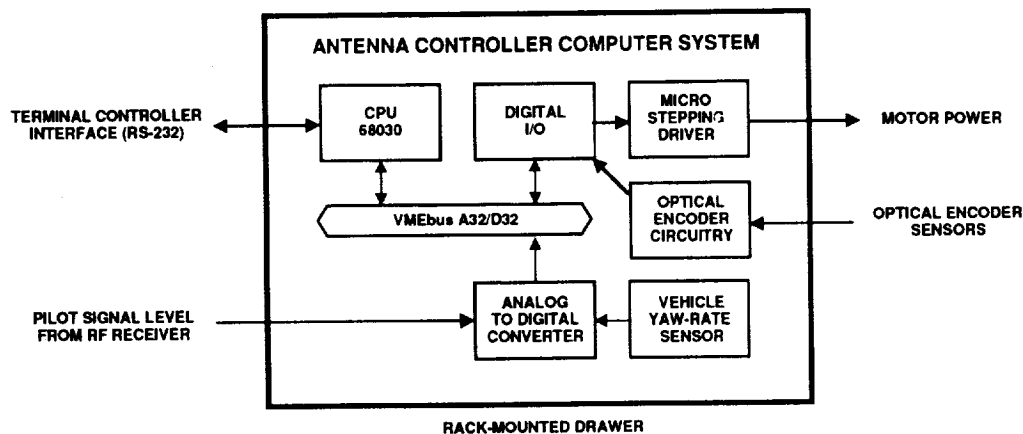
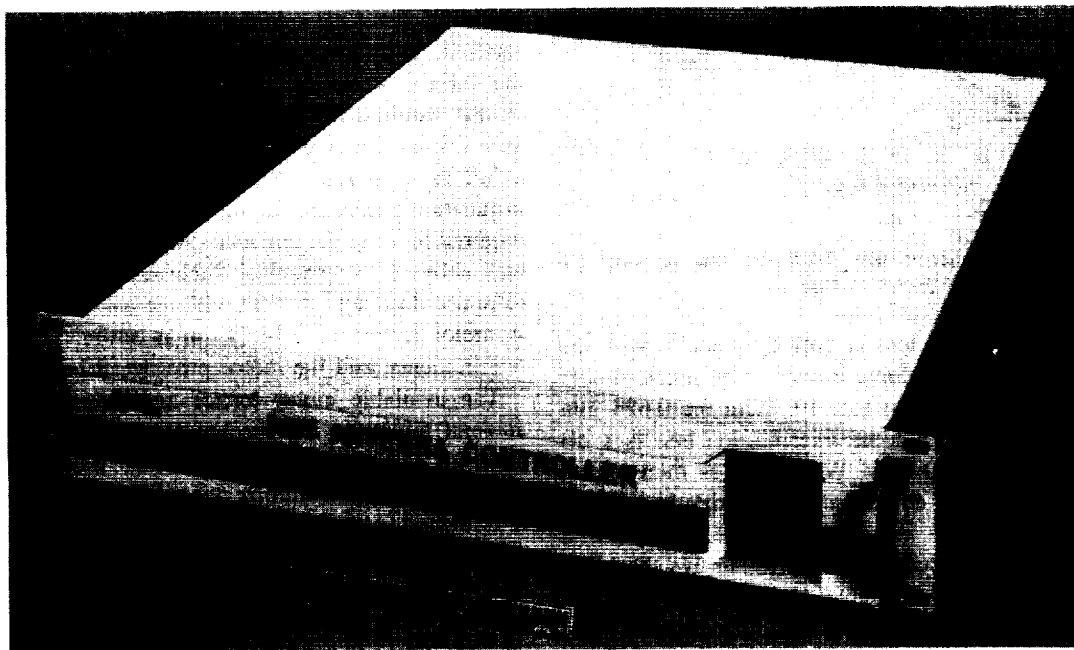Fig. 12. Antenna controller computer system block diagram.

Fig. 13. Antenna controller system.

continuously even if the vehicle is stationary. When the vehicle doesn't turn, the antenna doesn't turn, and the bearings dither in place. When this occurs, the bearing lubrication tends to work away from between the bearings and the surface they contact in the bearing race. To alleviate this, the antenna is rotated occasionally when the communications link is inactive and also a number of times during startup of the system to keep the bearing lubrication evenly distributed. Accounting for all of the abovementioned factors, the life of the motor bearings was estimated by analysis of the bearing load profile [31] and is estimated to be 3×10^6 hours—this exceeds the planned use of the AMT. The bearing load profile analysis assumes driving restricted to standard paved roads.

III. ANTENNA CONTROLLER

The antenna controller tracks the satellite as the mobile vehicle moves about. Tracking the satellite requires only azimuth steering (one-dimensional) since the antenna elevation coverage is wide enough to accommodate typical vehicle pitch and roll variations within any single geographical region of operation restricted to paved roads. The antenna controller steers the antenna azimuth angle in response to an inertial vehicle yaw-rate sensor and an estimate of antenna pointing error obtained by "mechanical dithering" of the antenna. The satellite tracking system is a custom-designed, turnkey, real-time imbedded microprocessor system, diagrammed in Fig. 12 and shown in Fig. 13. It mounts in a standard 48 cm wide rack drawer of 9 cm height.

The antenna tracking control system signal flow graph is shown in Fig. 14. Almost all that is required of the pointing system is to compensate for vehicle turns (yaw). The antenna pointing error is defined as the difference between the antenna motor angle, with respect to the vehicle, and the inertial vehicle yaw angle. This represents the fact that, with a very distant and stationary source (geostationary satellite), the direction to the source, as viewed from the vehicle, does not change significantly unless the vehicle turns.
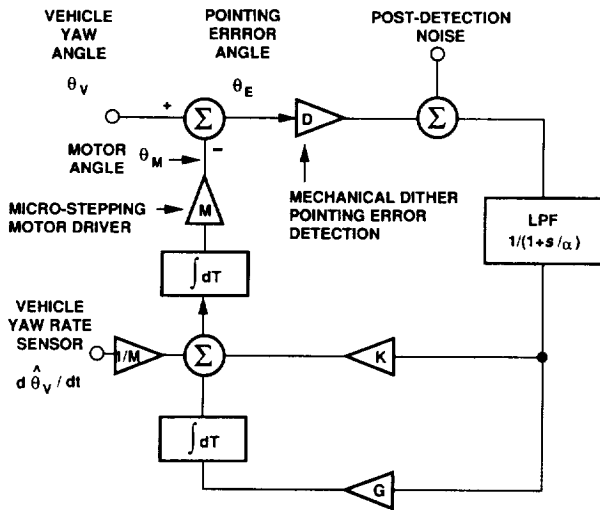
Fig. 14. Tracking system signal flow graph.

An inertial vehicle-yaw-rate sensor provides most of the information required to keep the antenna pointed at the satellite while the vehicle moves about, after an acquisition procedure determines the initial satellite direction. The yaw-rate sensor signal is integrated to yield an estimate of vehicle yaw angle, and the antenna is turned by this angle to counteract vehicle turns. Use of the full sensor bandwidth of about 70 Hz enables the antenna to respond quickly. There is no feedback in the yaw-rate sensor signal path. Any resulting pointing error is detected by the mechanical dithering process (feedback) and corrected by the tracking system.

Drift of the sensor bias is the most significant source of pointing error, and the tracking system must compensate for it. Since the sensor bias drifts very slowly, the resulting pointing error only very slowly has to be corrected. Only 0.1 Hz bandwidth of closed-loop feedback is sufficient to compensate for the inertial sensor bias drift. Minimizing the bandwidth of the closed-loop feedback is advantageous because of the accompanying flywheel effect and reduction in antenna jitter induced by noise in the pilot radio channel. The flywheel effect refers to the fact that the sluggish response of the low bandwidth feedback system tends to keep the antenna pointed at the satellite during short periods of signal outage, assuming proper yaw-rate sensor operation.

When the satellite is shadowed by an obstacle for a long time (> 30 s), such as when driving behind a building, the antenna may no longer be aligned with the satellite when the obstacle is cleared from the satellite view. The antenna system would then have to conduct an azimuth search to find the satellite again. The terminal controller, seen in Fig. 2, decides when to conduct the satellite search; the antenna system does not decide on its own.

If during a satellite search the direct line-of-sight satellite signal is blocked but a reflection is found (perhaps reflected from a building), the antenna may lock onto the reflected signal and attempt some communications if it is strong enough. The terminal controller would attempt to establish a communications link using the reflected signal but soon give up and conduct another search for the direct satellite signal. The

reasons for which the use of the reflected signal would be short are that a reflection has more severe signal dynamics in a mobile environment and thus more degraded communication quality than the line of sight. Parallax also quickly causes loss of the reflection because the antenna tracking system is trained on very distant sources—a reflection from a nearby building would be lost as soon as the vehicle drove away from the building.

A. Inertial Yaw-Rate Sensor:

The tracking system relies heavily on the performance of the vehicle-yaw-rate sensor. (Compare the use of 70 Hz bandwidth from the yaw-rate sensor to the tracking system 0.1 Hz closed-loop feedback bandwidth.) The rate sensor must thereby be suitably accurate, and on the short term provide all the information necessary to point the antenna properly. During short-term signal outages (less than 10 s), when loss of the pilot signal disables the tracking feedback, the rate sensor is the sole source of antenna pointing information. The sensor bandwidth must be at least about 50 Hz, so the delay in reaction to a change in vehicle yaw doesn't cause significant pointing error (> 0.5°). The yaw-rate sensor must also have good linearity, minimum scale-factor error, minimum noise, and minimum short-term bias drift. Long-term (slow) yaw-rate sensor bias drift—such as that imposed by temperature variations—is compensated by the antenna tracking system feedback and is thereby of little concern in the selection of a particular sensor for this application.

The turn-rate sensor utilized in the AMT design provides the required performance. It is of a small, quartz tuning-fork design. Its linearity is within 0.1%, and its scale factor error is less than 1%. Its noise represents an rms value of less than 0.05° and its bias drift is slow (< 5°/min.).
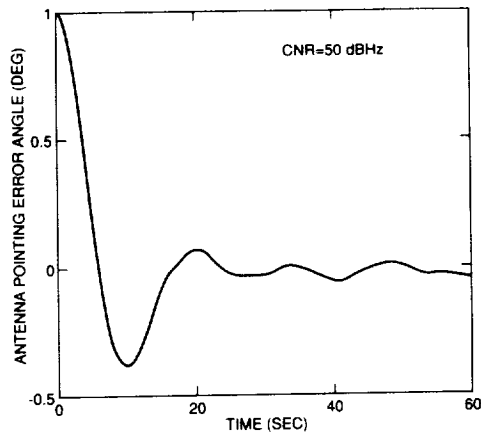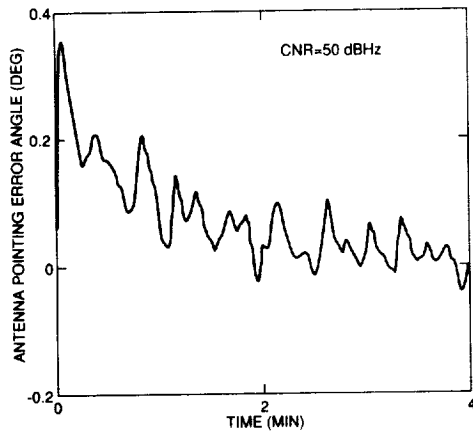
B. Tracking Control System:

The closed-loop control function, $F(s)$, which describes the response of the antenna angle to pointing error, in the Laplace s-domain, is given below along with an expression for the one-sided equivalent noise bandwidth (in Hz) of the closed-loop tracking control system. $F(s)$ is determined directly from Fig. 14, using Mason's rule for signal flow graphs.

$$F(S) \equiv \frac{\theta_M}{\theta_E}(S) = \frac{\alpha DKMs + \alpha DGM}{s^3 + \alpha s^2 + \alpha DKMs + \alpha DGM}$$

$$B_N \equiv \frac{1}{|F(0)|^2} \int_0^\infty |F(j\omega)|^2 \frac{d\omega}{2\pi} = \frac{DKM(K/G) + 1}{4(K/G - 1/\alpha)}$$

The design of the tracking control system involves the specification of the factors α, K, and G (the lowpass filter corner frequency and the two arbitrary system scale factors). The other two factors, D and M, are not arbitrarily chosen. The factor D represents the slope of the mechnical-dithering point-error-detection function, and it is discussed later. The factor $M = 1/45$ is a function of the motor design. The two-phase stepper motor with a 2° full-step angle has 45 electrical cycles per motor revolution.

The control system is designed for a slightly under-damped response with a closed-loop noise bandwidth of 0.1 Hz.

Fig. 15. Response to initial pointing error of 1°.

Fig. 17. Mechanical dithering pointing error detection function (coherent).

Fig. 16. Response to sudden rate sensor bias change of 0.1°/s.

The tracking system response to initial pointing errors, such as a residual acquisition error, is shown in Fig. 15. The classical slightly under-damped characteristic is evident, and the response time is seen to be approximately $1/B_N = 10$ s. The antenna pointing error in response to a sudden yaw-rate sensor bias change of 0.1°/s is shown in Fig. 16. The response time to such rate sensor bias fluctuations is the ratio K/G, 60 s in this case. Figs. 15 and 16 are the result of a simulation of the tracking system with a nominal pilot carrier-to-noise power spectral density ratio (CNR) of 50 dB · Hz. A lowpass filter corner frequency of 1 Hz is used, thus $\alpha = 2\pi$.

C. Mechanical Dithering:

The technique used to measure antenna azimuth pointing error and thus enable closed-loop tracking is mechanical dithering. Mechanical dithering involves rocking the antenna sinusoidally in azimuth angle 1° in each direction at a 2 Hz rate. The mechanical dithering causes less than 0.3 dB and 0.2° fluctuation of the signals (at the 2 Hz rate). The satellite sends a special pilot signal for antenna tracking. The AMT RF receiver detects the pilot signal through the antenna and reports the detected signal level to the antenna controller computer. By correlating the received pilot signal level reported by the receiver with the commanded dithering of the antenna angle, the antenna controller computer determines the sign and
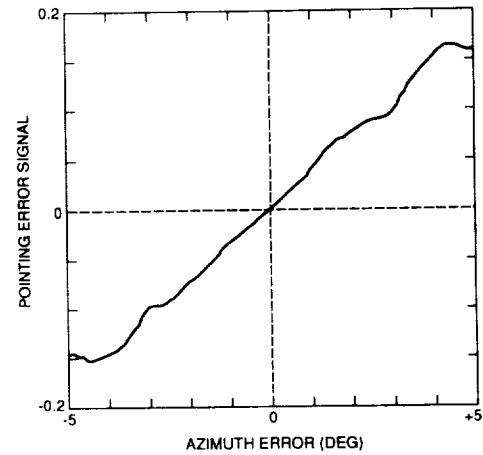
magnitude of any pointing error. Fig. 17 shows the measured mechanical dithering pointing error detection function with coherent detection of the pilot signal. (With noncoherent signal detection the shape of the function is the same but the slope is twice as large—but the post-detection noise spectral density is also at least 6 dB greater.) At large error angles, the function reveals a small nonlinearity in the motor. The measured slope of the function at the origin is about $0.035°^{-1}$, or 2.0 rad^{-1}, which agrees very well with calculations. This slope represents the factor D in the tracking control system signal flow graph of Fig. 14.

Antenna tracking using a monopulse technique was considered as an alternative to mechanical dithering but was not pursued because of the additional RF losses and feed complexity that monopulse circuitry introduces [32]. The phase shifters and greater circuit complexity required for monopulse impose additional significant RF losses at K and K_a bands (on the order of 2 dB) that are not imposed by mechanical dithering. Mechanical dithering requires no additional RF circuitry in addition to a basic antenna configuration with steering capability. The additional RF losses would reduce the antenna gain, increase the transmit power requirements, and increase the antenna noise temperature, thereby reducing receiver sensitivity.

To estimate pointing error using the mechanical dithering technique, the antenna controller makes the following computations while dithering the antenna. With the 2 Hz dither rate two estimates of pointing error are generated each second. Two values are accumulated during the dither cycle, and when each cycle is complete, the ratio of the two values yields an estimate of the current antenna pointing error. The denominator is simply the average pilot signal level received through the antenna during the dither cycle. The numerator is the difference between 1) a weighted average of the pilot signal level received while the antenna is dithered to one side, and 2) a weighted average of the signal level while the antenna is dithered to the other side. Proper choice of the weighting function reduces the relative variance of the pointing error estimate. In this application the optimum weighting (or windowing) function is a sinusoidal window which matches the dithering function; its use reduces the

variance by about 1 dB compared to a rectangular window.

The variance of the pointing error estimate is a function of the noise in the pilot channel. Since the pointing error estimate is the tracking system feedback source, the variance of the error estimate induces antenna pointing jitter, which is superimposed onto the normal movement of the antenna (vehicle yaw tracking and mechanical dithering). Antenna jitter is defined as random angular displacement of the antenna pointing angle (as seen in Figs. 15 and 16), induced by pilot radio channel noise and fading of the pilot signal (the mobile channel). With the nominal pilot signal CNR of 50 dB · Hz the rms antenna pointing jitter is 0.06°. Pointing jitter is significant only if greater than 0.5° rms, so there is a nominal margin of about 20 dB.

IV. CONCLUSION

A mobile vehicle antenna system for the K/K_a-band ACTS Mobile Terminal has been successfully developed by JPL, and laboratory tests show that the antenna and its satellite tracking system perform very well. It is small and rugged for operation in the mobile environment. It will be used for the first experimental use of the ACTS satellite soon after the satellite is operational, when the AMT will demonstrate voice, video and the data communication through the satellite from a mobile vehicle traveling along roads in southern California.

The antenna has a minimum transmit gain of 20.8 dBi at 30 GHz, and a minimum receive gain of 19.5 dBi at 20 GHz. It handles up to 10 W transmit power and provides a minimum receive sensitivity of −6 dB/K. The sidelobes are more than 20 dB down from the main lobe. Peak cross-polarization is no greater than −15 dB. The satellite tracking system compensates for vehicle yaw rates up to 60°/s. The rms pointing error while tracking is only a small fraction of a degree, and the antenna system is able to complete a full azimuth scan and acquire the signal in about five seconds.
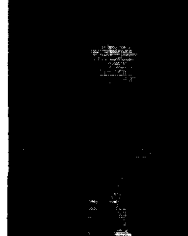
REFERENCES

[1] A. Densmore, V. Jamnejad, et al., "K/Ka-band antenna system for mobile satellite service," IEEE Antennas Propagat. Soc. Intern. Sym. Dig., June 1993.

[2] A. Densmore, V. Jamnejad, et al., "Two K/Ka-band mechanically steered, land-mobile antennas for the NASA ACTS mobile terminal," in Proc. Advanced Communications Technology Satellite Program Conference, NASA, Wash., D.C., Nov. 18–19, 1992.

[3] A. Densmore, V. Jamnejad, et al., "The ACTS mobile terminal reflector antenna system," SATCOM Quarterly, No. 7, JPL Publication No. 410-33-7, Oct. 1992.

[4] V. Jamnejad and A. Densmore, "A dual frequency K/Ka-band small reflector antenna for use in mobile experiments with the NASA advanced communications technology satellite," IEEE APS/URSI Joint Intern. Sym., URSI Digest, p. 1540, July 1992.

[5] A. Densmore and J. Huang, "A low cost, conformal antenna and tracking system for mobile satellite service," SATCOM Quarterly, No. 4, JPL Publication No. 410-33-4, Jan. 1992.

[6] A. Densmore, V. Jamnejad, et al., "Commercial applications of NASA's ACTS mobile terminal millimeter-wave antennas," in Proc Technology 2001 Conf., NASA JPL Publication D-9147, Dec. 1991.

[7] J. Huang and A. Densmore, "Microstrip Yagi array antenna for mobile satellite vehicle application," IEEE Trans. Antennas Propagat., vol. 39, pp. 1024–1030, July 1991.

[8] K. Woo, A. Densmore, et al., "Performance of a family of omni and steered antennas for mobile satellite applications," in Proc. Int. Mobile Satellite Conf. 1990, JPL Publication 90-7, June 1990.

[9] F. Colomb, et al., "An ANSERLIN array for mobile satellite applications," in Proc. Int. Mobile Satellite Conf. 1990, JPL Publication 90-7, June 1990.

[10] D. Bodnar, et al., "A novel array antenna for MSAT applications," IEEE Trans. Veh. Technol., vol. 38, pp. 86–94, May 1989.

[11] P. Estabrook and W. Rafferty, "Mobile satellite vehicle antennas: Noise temperature and receiver G/T," in Proc. IEEE Veh. Technol. Conf., San Francisco, CA, Apr. 1989.

[12] D. Bell, et al., "Reduced-height, mechanically steered antenna development," MSAT-X Quarterly, No. 18, JPL Publication 410-13-18, Jan. 1989.

[13] J. Berner and R. Winkelstein, "Antenna pointing system," MSAT-X Quarterly, No. 13, JPL Publication 410-13-13, Jan. 1988.

[14] V. Jamnejad, "A mechanically steered monopulse tracking antenna for land mobile satellite applications," in Proc. IEEE Veh. Technol. Conf., Tampa, FL, June 1987.

[15] J. Huang, "L-band phased array antennas for mobile satellite communications," in Proc. IEEE Veh. Technol. Conf., Tampa, FL, June 1987, pp. 113–119.

[16] D. Bell, "Antenna pointing schemes aim at high accuracy and robustness in a fading signal environment," MSAT-X Quarterly, No. 3, JPL Publication 410-13-3, June 1985.

[17] R. Emerson, "Propagation measurement van," MSAT-X Quarterly, No. 13, JPL Publication 410-13-13, Jan. 1988.

[18] J. Berner and R. Emerson, "The JPL MSAT mobile laboratory and the pilot field experiments," in Proc. Mobile Satellite Conf. 1988, JPL Publication 88-9, May 1988.

[19] A. Densmore, "Postperformance evaluation of the MSAT-X antennas used in the MSAT-X/AUSSAT land mobile satellite experiment," MSAT-X Quarterly, No. 24, JPL Publication 410-13-24, July 1990.

[20] K. Dessouky, et al., "Field trials of a NASA-developed mobile satellite terminal," in Proc. Int. Mobile Satellite Conf. 1990, JPL Publication 90-7, June 1990.

[21] W. Rafferty, "Mobile satellite field experiments," MSAT-X Quarterly, No. 11, JPL Publication 410-13-11, July 1987.

[22] J. Berner, "The PiFEx satellite-1a experiment," MSAT-X Quarterly, No. 15, JPL Publication 410-13-15, June 1988.

[23] T. Jedrey, et al., "The Tower-3 Experiment: An overview," MSAT-X Quarterly, No. 18, JPL Publication 410-13-18, Jan. 1989.

[24] T. Jedrey, et al., "An aeronautical-mobile satellite experiment," IEEE Trans. Veh. Technol., vol. 40, pp. 741–749, Nov. 1991.

[25] K. Dessouky et al., "The ACTS mobile terminal," SATCOM Quarterly, JPL Publication 410-33-2, July 1991.

[26] M. Sue, et al., "Personal access satellite system concept study," JPL Internal Document D5990, Feb. 1989.

[27] B. Levitt, "The ACTS mobile terminal rain compensation algorithm," SATCOM Quarterly, JPL Publication 410-33-2, July 1991.

[28] Y. T. Lo and S. W. Lee, Antenna Handbook. New York: Van Nostrand Reinhold, 1988, pp. 15–56.

[29] R. E. Collins, Field Theory of Guided Waves. IEEE Press, 1991.

[30] V. Jamnejad, "Radome studies for the AMT small reflector antenna," JPL Internal Document, IOM AMT:336.5-91-142, Feb. 1991.

[31] R. Blomquist, "Report of the mechanical analysis of the AMT antenna assembly," JPL Internal Document, IOM 3524-91-034, Feb. 1991.

[32] S. M. Sherman, Monopulse Principles and Techniques. Dedham, MA: Artech House, 1985.

Arthur C. Densmore (M'91) received the B.S.E.E. degree from California State Polytechnic University, Pomona, CA in 1986 and the M.S.E.E. degree from the California Institute of Technology, Pasadena, CA, in 1987.

Since 1987 he has worked at the Jet Propulsion Laboratory on the NASA Voyager-2 planet Neptune Radio Science experiment and the development of satellite-tracking land mobile vehicle antenna systems. He is currently developing two mobile vehicular antennas with microprocessor satellite-tracking control for NASA's Advanced Communications Technology Satellite Mobile Terminal experiment. His other research interests include communications, digital signal processing, real-time embedded microprocessor applications, and control systems.

Mr. Densmore is a member of the IEEE Vehicular Technology and Antennas and Propagation societies and *Tau Beta Pi*.

Vahraz Jamnejad (M'79) received the Ph.D. degree in electrical engineering from the University of Illinois at Urbana-Champaign in 1975, specializing in electromagnetics and antennas.

He was an assistant professor of electrical engineering at the Technical University of Tehran from 1975 to 1978, and a Visiting Professor at the University of Illinois from 1978 to 1979. He joined the Jet Propulsion Laboratory in 1979, where he has been engaged in research, software and hardware development, various areas of spacecraft antenna technology, and satellite communications systems. He has been involved in the study, design and development of ground and spacecraft antennas for future generations of Land Mobile Satellite Systems at L-band, Personal Access Satellite Systems at K and K_a bands, as well as feed arrays and reflectors for future planetary missions. His latest work on communications satellite systems involved the development of ground mobile antennas for NASA's ACTS mobile terminal satellite system. Presently, he is involved in research in parallel computational electromagnetics and studies on the applicability of large arrays of small aperture antennas for the NASA Deep Space Network. His general areas of interest and expertise include theoretical and numerical electromagnetics, microwave antennas, and Fourier optics.

Dr. Jamnejad is a member of *Sigma Xi* and *Phi Kappa Phi*.